

# Magnetic Concentrators for more Efficient Wireless Charging

Donovan Webb

Department of Physics, University of Bath, Bath BA2 7AY, United Kingdom

E-mail: dw711@bath.ac.uk

**Abstract.** A device capable of uniformly concentrating a magnetic field within a free space cavity will increase the efficiency of magnetic field sensing and wireless power transmission. A design for such a magnetic field concentrator, informed by the transformation optic technique, has previously been shown to concentrate static fields. However, for wireless power transmission, an oscillating magnetic field is required. Here we explore the efficacy of a magnetic concentrator, comprised of high permeability MuMetal and high conductivity copper, in oscillating fields with a specific focus on improving the efficiency of wireless power transmission. The device is shown to effectively concentrate both static and oscillating magnetic fields into its interior free space region by a factor of up to  $(3.0 \pm 0.1)$ . An almost 70 fold increase in the efficiency of wireless power transfer is shown when using a pair of magnetic concentrators. With the development of such devices, the convenience of wireless power transfer need not come at the cost of low efficiencies.

## 1. Introduction

The manipulation of magnetic fields is a critical tool for many modern technologies. Magnetic devices often have efficiencies dependent on the strength of interaction with an external magnetic field. Examples include energy harvesting from magnetic fields [1] to magnetoencephalography brain activity scans by locating small magnetic gradients [2]. The efficiency of such devices may be increased by concentrating the desired magnetic field within the area of sensing or harvesting.

Magnetic fields may be described by Maxwell's equations and are guided by materials due to their optical properties, such as permittivity and permeability. Snell's law allowed the design of many optical devices using geometrical lenses [3], however, with the maturation of fabrication techniques, many materials may be produced with exotic anisotropic optical properties [4] prompting the development of transformation optics (TO) — a modern approach to optical device design [5].

Here we describe one such TO designed device; The magnetic concentrator [6], with a particular focus on its efficacy in wireless power transmission. We first replicate static field concentration results [10] and then explore the benefits of the concentrating shells in both non-resonant and resonant near field wireless power transmission at various frequencies.

### 1.1. Transformation Optics and Metamaterials

TO informed the design of many new devices such as perfect lenses [7], magnetic-hoses [8], -cloaks [9], -rotators [9], and -concentrators [6]. It can be shown that due to the form invariance of Maxwell's equations, a spatial coordinate transform is equivalent to the insertion of a material with specific permeabilities and permittivities. This is shown conceptually by the three steps of the schematic shown in figure 1. First, a ray is considered in free Cartesian space in panel *a*, which due to Fermat's principle of least time will follow the horizontal spatial grid lines. The space is then transformed arbitrarily in panel *b* so that the ray adopts the desired path for the final device. The transformation

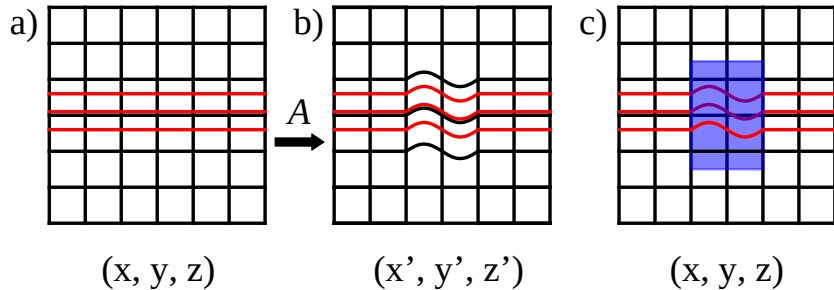


**Figure 1.** The steps of Transformation Optics. a) A ray (red) travelling in untransformed spatial coordinates (black grid) follows the path of least time. b) A spatial coordinate transformation  $A$  is applied to guide the ray along the desired path. c) A material (blue) is inserted into the untransformed space with corresponding permeabilities and permittivities which mimics the spatial coordinate transform  $A$  for the ray.

required,  $A$ , to morph the ray now informs the optical properties for the specific inserted material of panel *c*, which is once again located in untransformed space.

The form invariance of Faraday's law is described by the equivalent expressions

$$\nabla' \times \mathbf{E}' = -jw[\mu_0]\mathbf{H}' \quad \text{and} \quad \nabla \times \mathbf{E} = -jw[\mu']\mathbf{H}, \quad (1)$$

where the first is expressed in transformed coordinate space  $x'(x, y, z), y'(x, y, z), z'(x, y, z)$  and free space permeability  $[\mu_0]$ , whilst the second is expressed in untransformed Cartesian space  $x, y, z$  but with some space-dependent permeability  $[\mu']$ . Equivalent expressions exist for the remaining Maxwell equations and similarly some space-dependant permittivity  $[\epsilon']$  is required. The space dependant permeabilities and permittivities are found by

$$\mu' = \frac{A\mu_0 A^T}{|A|} \quad \text{and} \quad \epsilon' = \frac{A\epsilon_0 A^T}{|A|}, \quad (2)$$

where  $A$  is the Jacobian matrix describing the transformation of coordinate systems (e.g. between panel *a* and panel *b* in figure 1).

The resulting calculated optical properties may be anisotropic, have arbitrary magnitude and even have negative refractive index [7]. As bulk materials rarely, if ever, show these properties, optical metamaterials are often required [4].

Metamaterials are often comprised of repeating units whose dimensions are much smaller than the wavelength of the interacting radiation. The individual units may have specific geometry, orientation and optical properties to selectively interact with incident waves so that the net effect of the material mimics a bulk substance with different optical properties than its substituent parts.

### 1.2. Magnetic Concentrator

As described above, a device capable of magnetic field concentration can increase the efficiency of sensors and energy harvesters. Utilising TO we may design an optimal field concentrator which fulfils the following criteria: The magnetic field within a region  $A$  is concentrated into a cavity  $B$  where  $B$  is free space only. A possible geometry for this device that has cylindrical symmetry is shown on LHS of figure 2. To satisfy these conditions, two coordinate transforms are applied: First the region  $\rho < R_2 - \xi$  is radially and linearly compressed to the region  $\rho < R_1$ , where  $\xi$  is a thin 'skin' distance; Second, to ensure the continuity of our transformed space, a high ( $k^{th}$ ) order polynomial radial expansion of  $R_2 - \xi < \rho < R_2$  to the region  $R_1 < \rho < R_2$  is made. These transformations are described by the coordinate transformations

$$\begin{aligned} \rho' &= \frac{R_1}{R_2 - \xi}\rho, & \rho' \in [0, R_2 - \xi] \\ \rho' &= R_2^{1-k}\rho^k & \rho' \in [R_2 - \xi, R_2]. \end{aligned} \quad (3)$$

By symmetry we see that  $\theta$  and  $z$  remain unchanged through the two transformations. The corresponding Jacobians may be found for these transformations and using (2), the permeabilities of the required inserted material may be found to be

$$\begin{aligned}\mu' &= \begin{pmatrix} 1 & 0 & 0 \\ 0 & 1 & 0 \\ 0 & 0 & (\frac{R_2-\xi}{R_1})^2 \end{pmatrix} & \rho' \in [0, R_1) \\ \mu' &= \begin{pmatrix} k & 0 & 0 \\ 0 & 1/k & 0 \\ 0 & 0 & \frac{1}{k}(\frac{\rho'}{R_2})^{2/k-2} \end{pmatrix} & \rho' \in [R_1, R_2]\end{aligned}\quad (4)$$

Taking the limit  $\xi \rightarrow 0$  to concentrate all of the field within  $A$  into  $B$ , and matching the boundary conditions at  $R_2 - \xi$  and at  $R_1$ , we find that  $k \rightarrow \infty$ . From this we find that the required permeability within  $B$  is satisfied by free space whilst a material with radial permeability  $\mu_\rho \rightarrow \infty$  and angular permeability  $\mu_\theta \rightarrow 0$  is required for region  $A$ . The  $z$  components of permeability are ignored as we assume the cylindrical shell is infinitely long so the  $z$  component must be invariant. A model for this theoretical shell can be seen guiding an external magnetic field in the COMSOL simulation (figure 6a).

To satisfy these highly anisotropic conditions practically, an exploration of metamaterials is required. First, the relative magnetic permeability,  $\mu_r$ , of a material is defined by

$$\vec{B} = \mu_0 \mu_r \vec{H}, \quad (5)$$

where  $B$  is magnetic induction,  $\mu_0$  is vacuum permeability, and  $H$  is the externally applied magnetic field. If  $\mu_r$  is large (paramagnetic material) then the magnetic field density within the material is larger than the external field resulting in a “guiding” of field within the material’s interior. If  $\mu_r$  is small (diamagnetic material) then the field density is reduced within the material. A possible discretized shell construction is proposed [10] where the high radial permeability is provided by ferromagnetic materials whilst the angular permeability is shielded by superconducting material. MuMetal is a soft ferromagnetic material comprised of annealed nickel-iron alloy specifically created to possess unusually high permeability ( $\mu_r = 50,000 - 300,000+$ ). The magnetization of MuMetal responds to externally applied fields by the growth and shrinkage of individual magnetic domains. By annealing the MuMetal and removing defects, the individual domains may reshape rapidly in response to a magnetic field by the unimpeded movement of domain walls. By using thin sheets, the easy axis of magnetization also lies in-plane further enforcing the field to be guided within the sheets. Superconductors in their Meissner state ( $B = 0$ ) will exclude all magnetic fields from within their interior giving a relative permeability of 0. In an alternating field, a far cheaper option for blocking the angular magnetic field component is the use of high conductivity copper sheeting. From Lenz’s law, an oscillating magnetic field perpendicular to a metal sheet will induce eddy currents which will oppose the changing field. At an appropriate frequency, which is proportional to the copper thickness, the effective angular permeability is reduced to near zero. To approximate the conditions proposed by TO design, these two materials may be arranged in alternating angular sheets, as seen in figure 3.

In an external static uniform magnetic field, the ideal shell will increase the field within region  $B$  by a factor of  $R_2/R_1$ . Similarly, if a magnetic dipole is surrounded by the concentrating shell, then the field outside of the shell will be increased by a factor of  $R_2/R_1$ .

### 1.3. Wireless Power Transfer

The ability to transfer power between devices that are not connected by wires is useful in many settings: for convenience, e.g. charging mobile phones; for safety, e.g. implanted medical devices; or for practicality, e.g. satellites. We shall focus on near field power transmission by the use of inductive coupling. Inductive coupling transfers power between two coils of wire (two inductors) by an oscillating magnetic field. The transmitting coil is supplied with an alternating current, which by

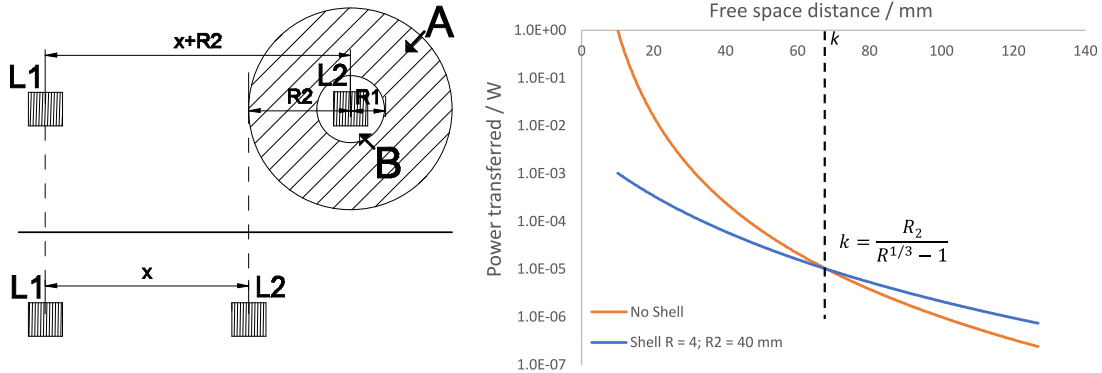


**Figure 2.** A concentrating shell with inner radius  $R_1$  and outer radius  $R_2$  is useful for increasing the efficiency of wireless power transmission by inductive coupling. Power transfer efficiency is highly sensitive to the distance between coils being proportional to  $r^{-6}$ . A concentrating shell increases this power transfer by  $(R_2/R_1)^2$  but at the cost of less free space,  $x$ , between the devices. However, at a critical distance  $k$ , the shell provides an improvement over bare dipoles for a given free space distance,  $x$ . LHS: The arrangement of two dipoles (boxes)  $L_1$  and  $L_2$  with a fixed free space gap  $x$ , either with a shell (Top) or without (Bottom). RHS: Theoretical power transfer plots for these two arrangements when the shell has  $R_2 = 40$  mm,  $R_1 = 10$  mm.

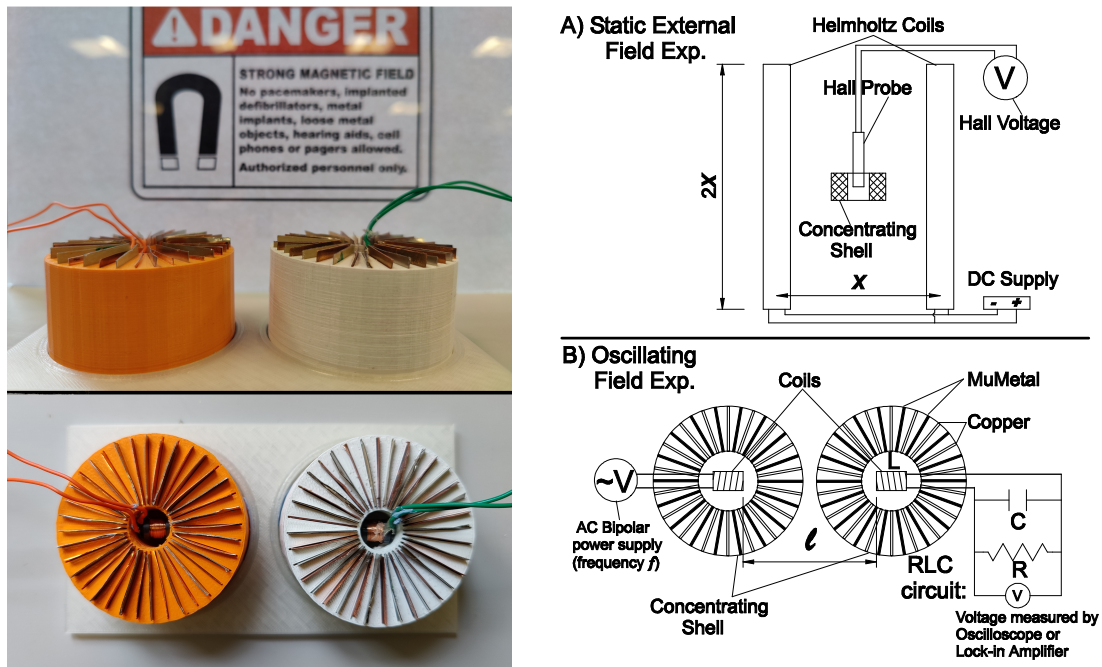


**Figure 3.** LHS: The constructed shells arranged in the power transfer experiment. RHS: A) The static field concentration experiment. Using a Hall probe to measure magnetic field within the inner radius of the shell when an external magnetic field is created by a pair of Helmholtz coils. B) The oscillating field concentration experiment (power transfer). A coil is driven by an AC power supply with a chosen frequency. A second coil is placed within the field of the first so a voltage is induced across it. A resonant RLC circuit is constructed incorporating the second coil to maximise power transfer.

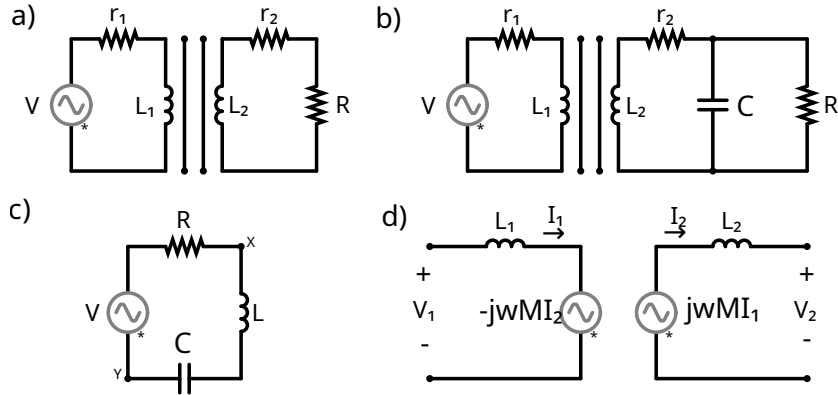


**Figure 4.** Wireless power transmission by inductive coupling. a) Simple circuitry for coupling  $L_1$  and  $L_2$  coils. The useful power transmitted is across load resistance  $R$  whilst power lost is across the internal resistance of coils,  $r_1$  and  $r_2$ . b) The receiving inductor is now part of a resonant RLC circuit. c) A series RLC circuit — when voltage at  $x$  and  $y$  are in phase, the resonant condition is met. d) An equivalent circuit to the coupled inductor circuits but with explicit induced voltages shown.

Ampere's law creates an oscillating magnetic field. The receiving coil is placed within this magnetic field so that a current is induced as described by Faraday's law. A schematic of these two coupled circuits can be seen in figures 4a, b, and d. This strategy for power transfer is highly sensitive to distance as the magnetic field of a point dipole drops off with distance cubed,  $r^{-3}$ , therefore the power is proportional to  $r^{-6}$  if the dipole is driven at a fixed frequency and current. If the dipole is a coil of wire with diameter  $d$  then this approximation holds only if  $r \gg d$ . The power transfer efficiency, PTE, also suffers with distance as the non-ideal resistive losses in the primary coil remain (relatively) constant with distance. To somewhat counteract this sharp drop off of efficiency with distance, concentrating shells may be used to magnify the transmitted field and locally concentrate the field around the receiving coil. The concentrating shell is larger than the coil by necessity, however, the presence of a shell is always advantageous when the free space distance between the power transmitting and power receiving device is greater than  $k$  [11], where

$$k = \frac{R_2}{\sqrt[3]{R} - 1} \quad (6)$$

and  $R$  is the ratio  $R_2/R_1$ . This arrangement and the critical distance  $k$  is shown in figure 2.

While the magnetic concentrating shells were designed by TO for static magnetic fields, in this work we explore their behaviour and efficacy in oscillating fields of a few kHz, which can be sufficient for practical power transfer [12].

## 2. Methods and Circuitry

### 2.1. Construction of shell

0.15 mm MuMetal (MSFHP from Thorlabs) sheets with  $\mu_r = 55,000 - 75,000$ , and 0.3 mm high conductivity copper sheets were cut into 21 mm by 30 mm rectangles. Plastic supports for holding 36 sheets of either MuMetal or copper were 3D printed to produce the shells seen in figure 3. The inner radius  $R_1$  and outer radius  $R_2$  were 7 and 28 mm respectively to give an  $R_2/R_1$  ratio of 4. The “Full shell” contains 36 sheets of alternating copper and MuMetal, whilst the “No shell” scenario contains no metal.

## 2.2. DC Magnetic Fields

Helmholtz coils (RHS figure 3) were powered by constant DC to create a uniform magnetic field within their center. A Hall probe placed at the center of the Helmholtz coils will have a Hall voltage induced which is proportional to the magnetic field. Once calibrated the Hall probe can be used to measure the absolute value of the magnetic field present. A concentrating shell may now be placed at the center of the Helmholtz coils and the Hall probe placed within the  $R_1$  section of the shells to explore field concentration.

## 2.3. Power Transfer

Power transfer experiments measure power dropped across a load resistor in a receiving circuit versus power lost in the transmitting circuit's inductor. The receiving circuit, seen in figure 4, has multiple arrangements to optimise power transfer, the simplest of which is the load resistor in series with the receiving inductor forming an RL circuit with no resonance conditions. Assuming the non-ideal real resistances of the coil is  $r_2 \ll \omega L$ , then the optimal load resistance for power transfer at some frequency  $\omega$  is found by,

$$\begin{aligned} V_2 &= I_2(j\omega L_2 + R), & (7) \\ P_R &= |I_2|^2 R = \frac{V_2^2 R}{\omega^2 L_2^2 + R^2}, & (8) \end{aligned} \quad \left| \begin{array}{l} \text{and setting } \frac{dP_R}{dR} = 0, \\ \Rightarrow R = \omega L_2. \end{array} \right. \quad (9)$$

The EMF induced in the receiving coil of a coupled inductance system may be found by Faraday's law,

$$\varepsilon = -\frac{d\phi_{21}}{dt}, \quad \text{or} \quad \varepsilon = -M \frac{dI_1}{dt}, \quad (10)$$

where  $\phi_{21}$  is the magnetic flux through coil 2 due to the current of coil 1 and  $M$  is the equivalent mutual inductance between two coils. If the current in coil 1 is alternating sinusoidally, then the maximum EMF induced in coil 2 will be  $MI_1\omega$ . Changes in mutual inductance for different shell constructions is a useful metric for field concentration as it is proportional to the magnetic flux present in coil 2. It may also be readily calculated if the current in coil one is known and the voltage across the load resistance in circuit 2 is measured at the optimal load resistance (see (9)). This simple relationship of voltage measurement  $V_2$  to mutual inductance  $M$  is described by

$$V_2 = \frac{MI_1\omega}{\sqrt{2}}. \quad (11)$$

It is well known that a resonant RLC arrangement on the receiving circuit can greatly increase the power transferred in inductive coupling [1]. At resonance the complex impedance of the inductance and capacitance cancel leaving only the load resistance. Our inductance is assumed to be identical between experiments as the same coils are used and the capacitance can be found to satisfy the resonance condition at a chosen operating frequency by the relationship

$$C = \frac{1}{\omega^2 L}. \quad (12)$$

Practically the resonant frequency and required capacitance were found using a resonant series RLC circuit as seen in figure 4c as this method was experimentally simple and fast. Resonance occurs in this circuit when  $V_x$  is in phase with  $V_y$ .

The parallel resonant RLC PTE arrangement is considered in figure 4b and may be simplified to the equivalent circuit in d, where the voltage across  $R_{load}$  is equal to,

$$V_2 = j\omega MI_1 - j\omega L_2 I_2, \quad \text{and} \quad I_2 = j\omega MI_1/Z_2, \quad (13)$$

where  $Z_2$  is the total impedance of circuit 2, which in the case of a parallel RLC circuit is equivalent to

$$Z_2 = j\omega L_2 + \frac{1}{j\omega C + R_{load}^{-1}}. \quad (14)$$

As with the non-resonant RL case, an optimal resistance must be found to maximise power transfer. In series RLC the optimal resistance is when  $R_{load}$  matches the sum of internal resistances of the components, however, in the parallel RLC case, it was found that the optimal resistance depended non-trivially on the internal resistances of the components, the frequency, and inductance/capacitance values. The internal resistances of the inductance was also found to be dependent on frequency further complicating the optimal resistance calculations. The optimal resistances were therefore found experimentally through a resistance sweep at each frequency. The load voltage can then be shown to be

$$V_2 = A \frac{MR_{opt}}{L_2} I_1, \quad (15)$$

where  $R_{opt}$  is the optimal resistance for power transfer and  $A$  is some constant. Surprisingly there is no explicit dependence of  $V_2$  on frequency, however, it was found that the optimal load resistance had an implicit dependence on frequency. All the parameters in this equation may be measured during a PTE experiment allowing the comparison of relative changes in mutual inductances (and equivalently magnetic fields) when different concentrating shells are used.

PTE was calculated by finding the power dropped across the load resistor in circuit 2 and dividing by the power dropped across the coil in circuit 1. An ideal inductance has voltage and current  $90^\circ$  out of phase meaning the time-averaged power loss is zero, however real inductors have non-ideal characteristics and so power may be found by,

$$P_1 = I_{rms1} V_{rms1} \cos(\phi), \quad (16)$$

where  $\phi$  is the phase difference between  $I_1$  and  $V_1$ .

### 3. Results

#### 3.1. DC Magnetic Fields

Using Helmholtz coils powered in DC to create a static external magnetic field (see Methods), we observed constant field concentration factors within the  $R_1$  cavity, across a range of external field strengths, for various shell constructions. No shell, 18 MuMetal, and 36 MuMetal shells were used and their concentration factor with field may be seen in figure 5a, where concentration factor,  $C$ , is defined as (Magnetic field within shell's cavity)/(external field produced by Helmholtz coils). It was found that the shell construction of 36 MuMetal thin sheets gave the optimum concentration factor of  $C_{36} = (2.43 \pm 0.04)$  with errors likely due to the sensitivity of dipole orientation within the field. The 18 MuMetal shell gave a magnetic concentration factor of  $C_{18} = (2.31 \pm 0.04)$ , which suggests that the shell behaves more ideally with a greater number of sheets. Simulation work performed on COMSOL further supports this difference between 18 and 36 MuMetal sheets as shown in figure 6e. The absolute values predicted by COMSOL,  $C_{18} = (2.32 \pm 0.01)$  and  $C_{36} = (2.46 \pm 0.02)$ , closely match the experimentally observed concentration factors for both cases.

#### 3.2. Power transfer

##### *Non-resonant power transfer using an RL circuit*

Power is transferred from the primary circuit to a load resistor in the secondary circuit in a coupled inductive arrangement as explained in Methods. This may be simply performed by placing a load resistor in parallel with the receiving inductor  $L_2$  forming an RL circuit with no resonant conditions as seen in figure 4a. To maximise power transferred, the optimal load resistance was matched to  $R = \omega L$  (see Methods (9)). Figure 5b shows the relative PTE versus load resistance for various frequencies confirming the expected optimum load resistance.

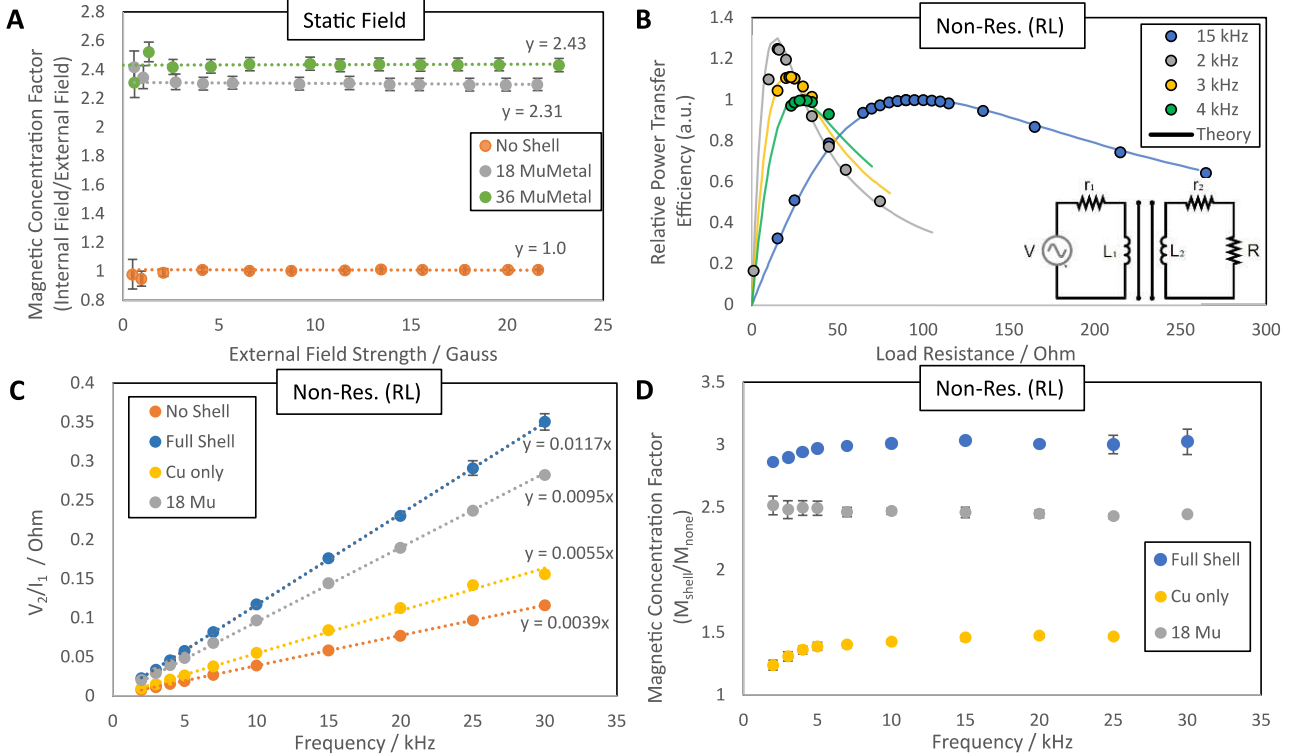


**Figure 5.** **A)** (DC) The concentration of external static fields into the interior cavity of shells comprised of either 18 or 36 MuMetal sheets. **B)** (AC) The dependence of relative power transfer efficiencies on load resistance in a coupled non-resonant RL inductive circuit for various frequencies. Points correspond to experimentally measured values whilst the solid lines are found using (8). **C)** Finding mutual inductance,  $M$ , between two coils at a fixed distance for various shell configurations in the non-resonant RL circuit arrangement. The gradient is equivalent to  $2\pi M/\sqrt{2}$  from (11). **D)** The shell's effect on mutual inductance is found by the ratio of ( $M$  with shell)/( $M$  bare coil). An increase in mutual inductance corresponds to an increase in magnetic field density within the shell and is shown to be dependant on frequency for shells with copper.

Mutual inductances between the coils (with inductances  $L \approx 1$  mH) at a set distance of 59 mm were found by: The voltage across the load resistor in the secondary RL circuit; the current driving the primary circuit, and using (11). The copper only, MuMetal only, and full copper plus MuMetal shells all showed a concentrating effect through their relative increases in mutual inductance between the two coils as shown in figure 5c. The full shell showed an increase of mutual inductance (magnetic field) by a factor of  $(3.0 \pm 0.1)$ , which is nearing the theoretical result from TO of  $R_2/R_1 = 4$  despite only containing 36 sheets. The frequency dependence on the relative increase in mutual inductance is shown in figure 5d. The two shell configurations containing copper are shown to have concentrating effects dependant on frequency. The concentrating effect rises steeply within the first 10 kHz and then plateaus for high frequencies. This expected behaviour initially motivated the choice for copper sheets in the shells for AC power transfer. At higher frequencies the perpendicular component of alternating magnetic fields produce eddy currents within the copper which, due to Lenz's law, oppose the change of field direction and effectively increases the angular permeability of the shell. Supporting work done on COMSOL (figure 6b – e) shows a similar observed effect where 36 copper sheets increases the concentration factor rapidly from  $C = 1$  at 0 Hz to  $C \approx 1.5$  by 10 kHz and then only a small further increase in efficacy at higher frequencies.

Apart from errors due to instrument, measurement reading, and coil placement, we observed noise due to stray magnetic fields inducing pick-up within cables connecting the coil to the lock-in

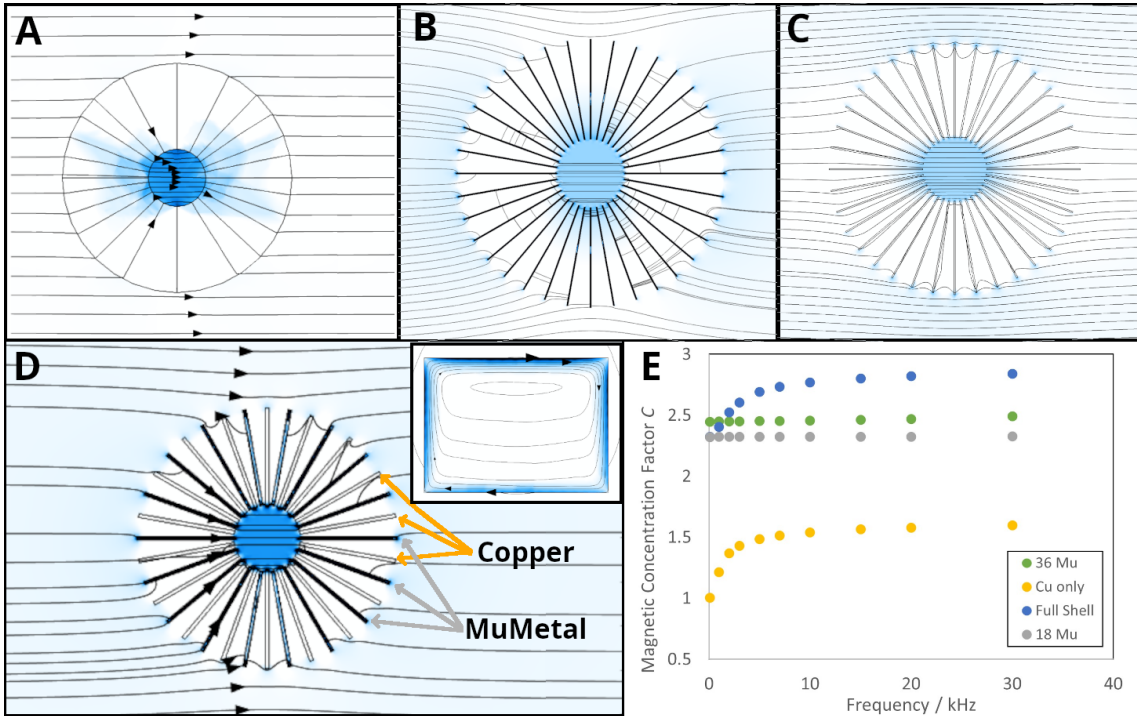


**Figure 6.** Exploration of magnetic field distributions using the COMSOL Multiphysics simulation package. **A)** The perfect anisotropic shell, designed by TO with infinite radial permeability and zero angular permeability, in a static external magnetic field. **B)** A MuMetal only shell guiding a static field. Note the field is guided radially through the interior of the MuMetal but angular field is not adequately blocked. **C)** A copper only shell guiding an oscillating external magnetic field (30 kHz) by effectively shielding the angular component by the production of eddy currents. **D)** A full shell comprised of alternating 18 MuMetal and 18 copper sheets in an oscillating external magnetic field (20 kHz). The dimensions of the simulated shell match those of the real fabricated shells. The MuMetal sheets are darker due to guiding the field within their interior whilst the copper sheets deflect the angular component of the fields. The inset image displays the eddy current density within a copper sheet when an oscillating magnetic field is applied at 45°. **E)** The dependence of magnetic concentration factor ((field within cavity)/(external field)) of various shells on frequency of the oscillating field. It can be seen that the two shells with copper show improved concentration as frequency is increased as predicted and also shown experimentally.

amplifier. This source of noise is highly frequency-dependent and is at the same frequency as our desired signal, so could not be removed by the use of a lock-in amplifier. To suppress this noise, cable placement was carefully managed and EM shielding was installed.

#### Resonant power transfer using an RLC circuit

Resonant parallel RLC circuits are more fitting for optimising power transfer (see Methods). For the arrangement described in figure 4b, a full shell comprised of 18 MuMetal and 18 copper sheets was explored. The optimal load resistances were found experimentally by measuring power for a sweep of resistances, an example of which is shown in figure 7a for a field frequency of 30 kHz.

From (15), the voltage measured across the load resistor is proportional to the mutual inductance between the two coils when the optimal load resistor is used, and the resonance condition for the RLC circuit is met. Figure 7b confirms this relationship and shows an increase in mutual inductance when the full concentrating shell is present. The gradient was found to be increased by a factor of  $(2.6 \pm 0.2)$  corresponding to a field concentration of the same factor if the inductance of  $L_2$  is assumed

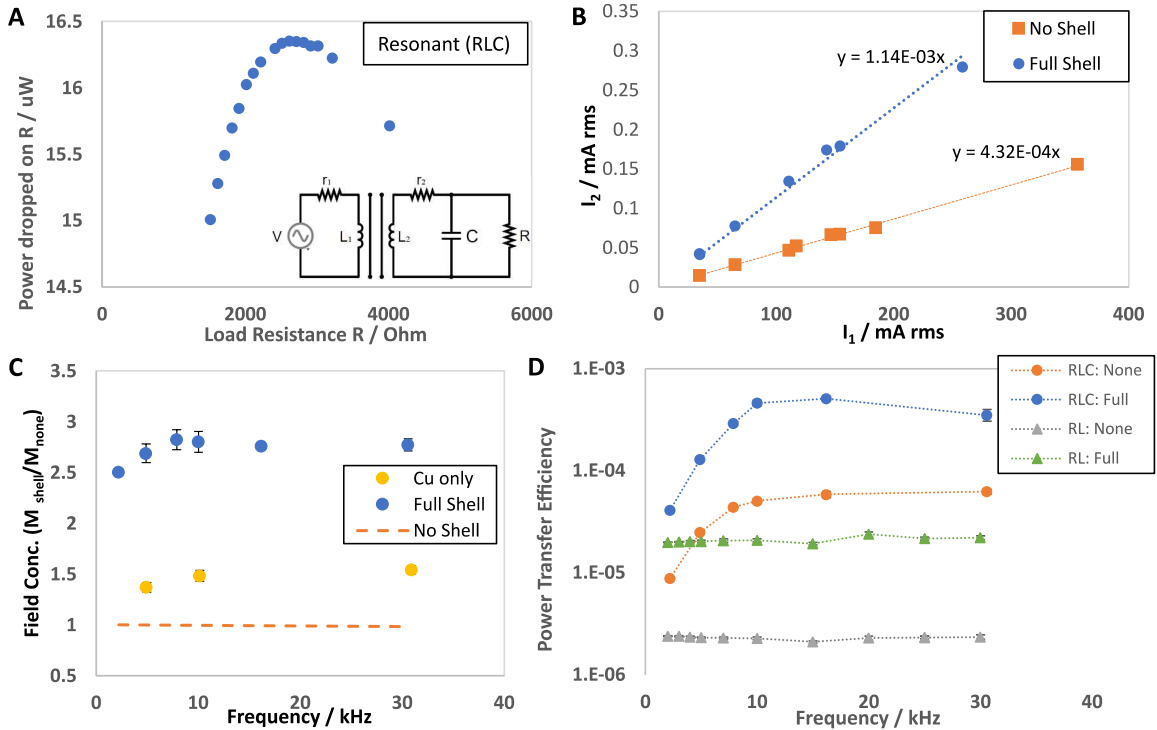


**Figure 7.** **A)** Locating the optimal load resistance for power transfer in a resonant parallel RLC receiving circuit at an AC frequency of 30 kHz. **B)** The current across the optimal load resistance is proportional to mutual inductance in the resonant parallel RLC circuit as seen in (15). Voltage across the transmitting coil remained constant and so various  $I_1$  were achieved by using different resonant frequencies. Comparing the gradients of  $I_2$  against  $I_1$  for the case when a shell is present to when one is not gives the factor increase of mutual inductance which is equivalent to the concentration of the field within the shell. **C)** The shell’s effect on mutual inductance in an RLC circuit is found by the ratio of ( $M$  with shell)/( $M$  bare coil). As with the RL circuit, the concentration of field is dependant on frequency for the full shell which has copper present. **D)** A comparison of power transfer efficiencies (PTE) for both a full shell (18 copper and 18 MuMetal sheets) and no shell in either the non-resonant RL or resonant RLC case. PTE is given as a ratio of power dropped across the load resistor against power lost in the transmitting coil as explained in Methods.

to remain constant (see Discussion).

The dependence of frequency on concentration factor is shown in figure 7c and it can be seen that, as with the non-resonant RL and simulated experiments, the presence of copper in the shell leads to a low initial concentration which increases with frequency until around 10 kHz at which point the concentration factor plateaus.

The PTE for non-resonant RL and resonant RLC, no shell and full shell arrangements are compared in figure 7d. It can be seen that the shell increases the efficiency in both cases by a similar factor and that the parallel resonant RLC arrangement gives a much greater efficiency than using the simpler RL circuitry. The optimal power transfer efficiency achieved at 30 kHz and 59 mm with one “full” shell was  $(0.035 \pm 0.005)\%$ .

A second “full” shell with the same dimensions was placed around the transmitting coil (seen in figure 3) and this further increased PTE to  $(0.35 \pm 0.02)\%$ . This second shell gave a power increase of around a factor of 10 which corresponds to a further field concentration of  $\sqrt{10} \approx 3.2$ . To explore the efficacy of this approach at closer distances the two coils were separated by 49 mm yielding a PTE of  $(0.015 \pm 0.004)\%$  with no shells and  $(1.0 \pm 0.1)\%$  with two full shells. The use of two concentrating shells displayed an almost 70 fold increase in efficiency.

#### 4. Discussion

For the constructed shells used in these experiments, their  $R_2/R_1$  ratio was  $(4.0 \pm 0.2)$  and from the theoretical TO work, it was predicted that the field should be concentrated in the perfect shell by the same ratio. The greatest concentration of field we observed was  $C_{full} = (3.0 \pm 0.1)$  in the AC non-resonant RL case. This concentration is still well below the expected theoretical concentration factor of  $C = (4.0 \pm 0.2)$  and likely explained by our approach to approximating the perfect TO designed anisotropic shell to a discretized version comprised of sections of high and low permeability. In both static and oscillating fields, experimentally and in simulations, we found that 36 MuMetal sheets performed better than 18 MuMetal sheets which suggests that finer discretization of the proposed shells gives concentrations closer to the theoretical value. Furthermore, in the static field experiments, only air was used to approximate the zero relative angular permeability. Air has a permeability of  $\mu_r \approx 1$ , which although is far less than the MuMetal's  $\mu_r = 55,000 - 75,000$ , is likely still a poor approximation. This can be seen by the increase in performance in the oscillating external field experiments where copper sheets are introduced to effectively screen out angular field density by the production of eddy currents.

Previous work by Prat-Camps *et al.* (2014) [10] included the exploration of MuMetal and superconducting (SC) shells for concentrating static magnetic fields. This work quoted a concentration factor of 2.70 at temperature below  $T_c$  for the SC material and 2.23 above the critical temperature for a shell of the same dimensions as explored here. These values agree well with our determined concentrations for 18 and 36 MuMetal sheets and emphasises the need for restricting angular field through the increase of concentration when SC is present. This parallels our findings of copper's effectiveness in increasing concentration in the oscillating field. The use of copper also has the benefit of room temperature operation being possible however, its practicality is strictly limited to frequencies above which eddy current generation is sufficient to shield angular fields.

We assumed the inductance of the coil was independent of the shell surrounding it, however, from finding resonance for each experiment using (12) we observed that the presence of a MuMetal shell significantly changed the inductance of the coil. The bare coil, and when surrounded by a copper only shell, gave an inductance of  $(1.02 \pm 0.02)$  mH whilst the coil surrounded by the full shell was found to be  $(1.25 \pm 0.01)$  mH. This increase in inductance can be understood by the high permeability MuMetal in the shell being located near to the coil, which increases the relative permeability of space in the vicinity of the coil. A change in inductance of coil 2 is important in the calculation of mutual inductance as shown in (15), and if accounted for, gives concentration factors of  $C_{full} = (3.1 \pm 0.2)$  in the resonant RLC case which is in closer agreement to the concentration observed in the non-resonant RL experiments. An increase in inductance may also lead to a decrease in PTE depending on the relationship between  $R_{optimal}$  and inductance in the resonant RLC circuit, but this could be avoided by increasing the distance between the coils and the MuMetal sheeting of the shell.

The poor PTE in all cases is explained by our choice of a ferrous core coil 1. This choice was motivated by the sensitivity of our detection equipment, the limitations of the current we were able to supply to our coils (greater current gives greater  $B$  field), and the limitations of the coil radius as it must fit within our shells. The ferrous-core solenoid had a relatively large non-ideal character with a measured phase difference between current and voltage being consistently between  $80^\circ$  and  $85^\circ$  depending on the frequency and absolute value of current being supplied. Using a more ideal inductor would greatly improve PTE and would be necessary if this device were to be used in a practical setting. A laminated core inductor could also give greater PTE whilst still maintaining a relatively high inductance value as this would reduce the production of eddy current losses within the inductor's core as operating frequency is increased.

#### 5. Conclusions

We have shown a proof of concept for the use of transformation-optics designed magnetic concentrating shells in wireless power transmission. Previously such shells have been shown to

concentrate static magnetic fields, which is useful in magnetic field detection, however here we have extended this work and explored the efficacy of shells in concentrating oscillating fields with frequencies up to 30 kHz. We experimentally found that our fabricated 36 sheet MuMetal shells performed similarly in both static and oscillating fields giving a  $(2.4 \pm 0.1)$  factor increase in magnetic field. In the oscillating regime we demonstrated the ability of copper sheets to effectively guide magnetic fields in the concentrating shell, their dependence on frequency and their overall increase in field concentration over just MuMetal. With two shells comprised of MuMetal and copper sheets only we showed an improvement on the efficiency of near-field power transmission by almost 70 fold over a distance of 49 mm at a frequency of 30 kHz.

In future work, to make such a power transfer device more practical, larger elliptical coils could be used within both shells allowing the generation and harvesting of stronger magnetic fields with a supplied current. Such coils may be narrow to minimise  $R_1$ , but extend in the  $z$ -direction of the shells to increase the area of one wire loop.

The effectiveness of these MuMetal and copper shells should also be explored in the MHz frequency range as is required by some high efficiency power transmission strategies [13]. As the permeability of MuMetal may drop substantially at this field frequency, other less frequency-dependent materials may need to be sought to create effective magnetic concentrators.

## 6. Acknowledgements

I would first like to thank my project partner Dominic Wildman for all his contributions to the success of this project and especially for his focus and drive with the COMSOL simulations work. I also thank Professor Simon Bending for his continual support throughout the project and for his guidance both in theory and experimental work. Finally, thanks to the University of Bath Physics Lab and workshop staff for their help with equipment and in fabricating the shells.

## 7. References

- [1] J. Hirai, T.-W. Kim, and A. Kawamura, “Wireless transmission of power and information and information for cableless linear motor drive,” *IEEE Transactions on Power Electronics*, vol. 15, pp. 21–27, 1 2000.
- [2] D. Cohen, “Magnetoencephalography: Evidence of magnetic fields produced by alpha-rhythm currents,” *Science*, vol. 161, pp. 784–786, 8 1968.
- [3] J. B. Pendry, A. Aubry, D. R. Smith, and S. A. Maier, “Transformation optics and subwavelength control of light,” *Science*, vol. 337, pp. 549–552, 8 2012.
- [4] D. R. Smith, J. B. Pendry, and M. C. K. Wiltshire, “Metamaterials and negative refractive index,” *Science*, vol. 305, pp. 788–792, 8 2004.
- [5] J. B. Pendry, D. Schurig, and D. R. Smith, “Controlling electromagnetic fields,” *Science*, vol. 312, pp. 1780–1782, 6 2006.
- [6] C. Navau, J. Prat-Camps, and A. Sanchez, “Magnetic energy harvesting and concentration at a distance by transformation optics,” *Physical Review Letters*, vol. 109, 12 2012.
- [7] J. B. Pendry, “Negative refraction makes a perfect lens,” *Physical Review Letters*, vol. 85, pp. 3966–3969, 10 2000.
- [8] C. Navau, J. Prat-Camps, O. Romero-Isart, J. Cirac, and A. Sanchez, “Long-distance transfer and routing of static magnetic fields,” *Physical Review Letters*, vol. 112, 6 2014.
- [9] F. Sun, B. Zheng, H. Chen, W. Jiang, S. Guo, Y. Liu, Y. Ma, and S. He, “Transformation optics: From classic theory and applications to its new branches,” *Laser and Photonics Reviews*, vol. 11, 11 2017.
- [10] J. Prat-Camps, C. Navau, and A. Sanchez, “Experimental realization of magnetic energy concentration and transmission at a distance by metamaterials,” *Applied Physics Letters*, vol. 105, 12 2014.
- [11] J. Prat-Camps, C. Navau, and Sanchez, “Quasistatic metamaterials: Magnetic coupling enhancement by effective space cancellation,” *Advanced Materials*, vol. 28, pp. 4898–4903, 6 2016.
- [12] C.-S. Wang, O. Stielau, and G. Covic, “Design considerations for a contactless electric vehicle battery charger,” *IEEE Transactions on Industrial Electronics*, vol. 52, pp. 1308–1314, 10 2005.
- [13] A. Kurs, A. Karalis, R. Moffatt, J. D. Joannopoulos, P. Fisher, and M. Soljacic, “Wireless power transfer via strongly coupled magnetic resonances,” *Science*, vol. 317, 7 2007.